

Repulsor: Accelerating Generative Modeling with a Contrastive Memory Bank

Shaofeng Zhang^{1*†}, Xuanqi Chen^{1*}, Ning Liao^{2*}, Haoxiang Zhao¹
 Xiaoxing Wang², Haoru Tan³, Sitong Wu⁴, Xiaosong Jia⁵, Qi Fan⁶, Junchi Yan²
 sfzhang@ustc.edu.cn, yanjunchi@sjtu.edu.cn

¹School of Artificial Intelligence and Data Science, University of Science and Technology of China,
² Shanghai Jiao Tong University, ³HKU, ⁴CUHK, ⁵Fudan University, ⁶Nanjing University



Abstract

The dominance of denoising generative models (e.g., diffusion, flow-matching) in visual synthesis is tempered by their substantial training costs and inefficiencies in representation learning. While injecting discriminative representations via auxiliary alignment has proven effective, this approach still faces key limitations: the reliance on external, pre-trained encoders introduces overhead and domain shift. A dispersed-based strategy that encourages strong separation among in-batch latent representations alleviates this specific dependency. To assess the effect of the number of negative samples in generative modeling, we propose Repulsor, a plug-and-play training framework that requires no external encoders. Our method integrates a memory bank mechanism that maintains a large, dynamically

updated queue of negative samples across training iterations. This decouples the number of negatives from the mini-batch size, providing abundant and high-quality negatives for a contrastive objective without a multiplicative increase in computational cost. A low-dimensional projection head is used to further minimize memory and bandwidth overhead. Repulsor offers three principal advantages: (1) it is self-contained, eliminating dependency on pretrained vision foundation models and their associated forward-pass overhead; (2) it introduces no additional parameters or computational cost during inference; and (3) it enables substantially faster convergence, achieving superior generative quality more efficiently. On ImageNet-256, Repulsor achieves a state-of-the-art FID of **2.40** within 400k steps, significantly outperforming comparable methods.

^{*}: Equal contribution. [†]: Corresponding author

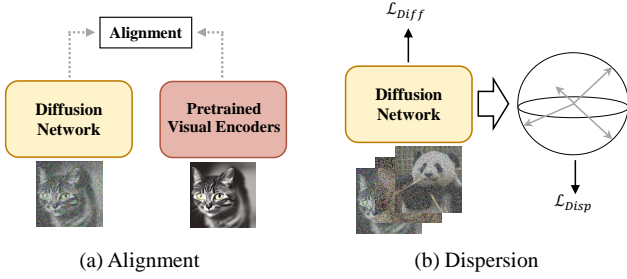


Figure 1. Two primary strategies for incorporating discriminative representations into the training of diffusion models: (a) Representation alignment guided notably by an external pre-trained encoder, exemplified by REPA [60]; and (b) Positive-free contrastive regularization, as previously introduced in disperse [55].

1. Introduction

In recent years, generative models operating on denoising principles, such as diffusion [14, 27, 47, 50, 51] and flow-based [19, 33, 36, 37] models, have become the predominant and scalable paradigm for high-dimensional visual modeling. They have demonstrated exceptional performance in core applications, including video generation [5, 18, 43], text-to-image synthesis [45, 47, 48], and image generation [29, 63]. However, substantial training costs and bottlenecks in representation learning efficiency continue to impede further progress. A promising and validated approach to address these limitations involves incorporating an auxiliary representation learning task. This method aligns the intermediate features of the generator with a semantically rich and structurally robust representation space, which serves to regularize the feature manifold and ease the optimization process, especially during the early training.

Self-supervised contrastive learning [4, 6, 10, 11, 21, 24, 61, 62] leverages data augmentation to construct positive pairs from augmented views of the same instance, while views from different instances serve as negative samples. The learning process is driven by optimizing an InfoNCE-based objective [53], which encourages the model to attract positive pairs in the embedding space while repelling negative ones. This paradigm results in representations that are not only semantically discriminative and linearly separable but also demonstrate fast convergence speed [25, 57].

To speed up the training of diffusion models, recent efforts to inject discriminative representations into diffusion training have progressed along two directions (see Figure 1): alignment [7, 34, 35, 54, 58–60] and dispersion [55]. REPA [60] introduces an auxiliary alignment loss without modifying the primary objective, mapping noisy intermediate features into the clean semantic space of a large self-supervised encoder, which stabilizes early optimization and accelerates convergence. Although REPA substantially improves training efficiency and generative quality, important

limitations persist: REPA relies on an external, pre-trained encoder, which increases forward-pass overhead and introduces the risk of domain shift. To address this limitation, inspired by negative pair-based contrastive learning, another line based on disperse [55] objective is proposed, which adopts contrastive regularization without positives, encouraging strong separation among in-batch latent representations in feature space to prevent collapse, while remaining jointly optimizable with the diffusion objective.

A substantial body of work has established that the number of negative samples is pivotal in contrastive learning: more negative pairs strengthen InfoNCE and yield stronger representations [24, 31]. Building on negative-based dispersive loss for generative modeling, we ask: **Does an analogous scaling law hold for generative models with respect to the number of negative pairs?** However, simply scaling the mini-batch to harvest more negatives conflicts with our goal of efficient and accessible training and often incurs multiplicative cost [9]. We therefore propose Repulsor, which decouples the effective number of negatives from the current mini-batch by maintaining a large, dynamically updated queue-based memory bank across iterations. A lightweight projector is further introduced to map features into a low-dimensional space, reducing memory and bandwidth while preserving discriminative capacity. Our Repulsor has three main advantages:

i) Repulsor does not rely on any pretrained vision foundation model (e.g. DINO v2 [42]). By leveraging a memory bank together with a low-dimensional projection head, it constructs abundant and high-quality negatives, learns discriminative representations directly within the generator, and avoids the forward pass overhead and domain shift risks introduced by external encoders.

ii) Repulsor introduces no additional parameters or computation at inference. The memory bank and the projection head are used only during training as auxiliary objectives, and the inference path is identical to the baseline.

iii) Repulsor converges substantially faster than existing methods [39, 55]. Under the same training configuration, it reaches superior generative quality earlier. Concretely, on ImageNet-256 it achieves **2.40 FID** within 400k steps (w/ CFG), surpassing disperse at 5.09 and SiT at 6.02.

2. Related Work

Self-Supervised Learning Self-supervised learning (SSL) in computer vision aims to exploit large collections of unlabeled images by designing proxy signals for pretraining, enabling models to acquire transferable and discriminative representations without manual annotations. Contemporary SSL methods largely fall into two families: contrastive learning (CL) [6, 10, 21, 24] and masked image modeling (MIM) [4, 11]. CL methods optimize instance-level invariance by maximizing agreement between embeddings

of different augmentations of the same image while pushing apart others, thereby uncovering structure in unlabeled data. Representative approaches include SimCLR [9], which emphasizes strong data augmentation with a simple objective, DINO [62], which adapts self-distillation to the unlabeled regime, and Rank-N-Contrast (RNC) [61], which introduces a ranking-based objective grounded in sequential representation learning. In contrast, MIM corrupts images by masking patches and trains models to reconstruct the missing content from visible context, encouraging the learning of semantically rich features. MAE [25] is a canonical example, employing a lightweight autoencoder to reconstruct masked regions. Building on this paradigm, subsequent work proposes new pretraining designs [1, 57] and explores alternative reconstruction targets and objectives [2, 17, 56].

Diffusion Models Recent generative diffusion methods are predominantly categorized into two classes: Diffusion Probabilistic Models (DPMs) and Flow Matching (FM). DPMs [14, 27, 41, 47, 50, 51] perform generative modeling by progressively diffusing data into Gaussian noise and learning the reverse denoising process. They have demonstrated exceptional performance in diverse tasks, including unconditional video generation [5, 18, 43], text-to-image synthesis [45, 47, 48], text-to-video generation [5, 22], and conditional image generation [29, 63]. FM [36, 37] has emerged as a powerful alternative, offering faster sampling speeds while achieving sample quality comparable to DPMs [12, 19, 33, 36, 44]. As a flow-based generative model, it estimates a transformation from a prior distribution (e.g., Gaussian) to the target data distribution. Unlike normalizing flows [16, 46], which directly estimate the noise-to-data mapping under specific architectural constraints, FM employs flexible architectures to regress a time-dependent vector field that generates the flow by solving the corresponding ordinary differential equation (ODE) [8].

Representation Learning as Regularization for Diffusion In the context of image generation, a recent line of work has explored representation learning as a form of regularization for diffusion models. REPA [60] explicitly injects external priors by aligning the intermediate representations of the generator with those from a frozen, high-capacity, pre-trained encoder, which can be trained on external data with diverse objectives. Building on this, SARA [7] integrates structured and adversarial alignment to enforce multi-level, fine-grained representation consistency. U-REPA [54] adapts this concept to the diffusion U-Net, mitigating the spatial-semantic mismatch via MLP upsampling and manifold constraints. REPA-E [35] enables end-to-end joint optimization of a VAE and a Latent Diffusion Model (LDM), introducing a differentiable normalization layer to stabilize statistical propagation between them. For cross-modal text-to-image alignment, SoftREPA [34] employs soft text tokens and contrastive learning to enhance

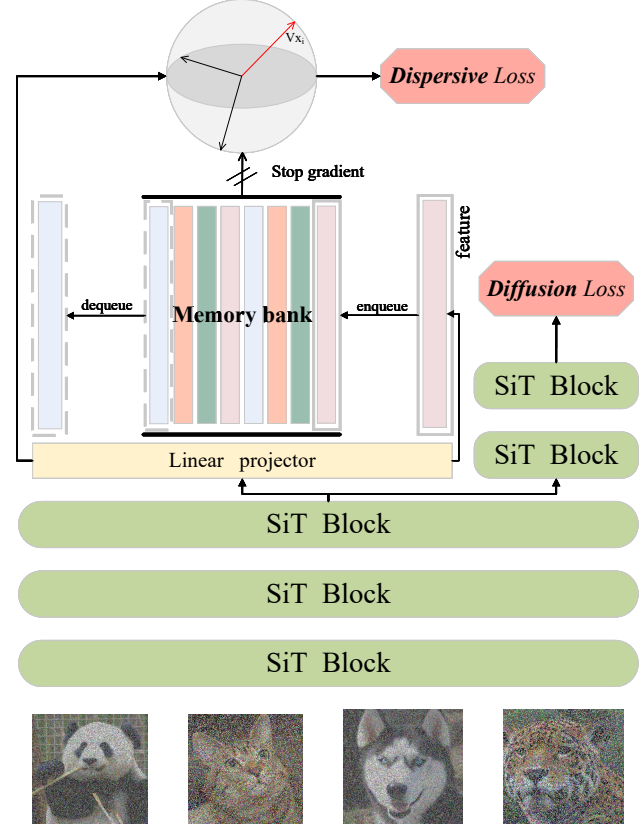


Figure 2. Framework of the proposed Repulsor. We introduce the Repulsor loss into the intermediate layers of denoising-based generative models (e.g., diffusion and flow-matching) to accelerate training convergence. By integrating a memory bank with a low-dimensional projection head, our approach decouples the effective negative sample size from the mini-batch size. This design significantly enriches the diversity of negative samples and strengthens the optimization signal, thereby enhancing feature separability.

semantic consistency and editability. VA-VAE [59] reconstructs the latent variable structure from its foundations, significantly accelerating the convergence of subsequent Diffusion Transformers (DiTs). disperse [55], in turn, enhances the diversity and fidelity of generated outputs by encouraging the dispersion objective of internal representations.

3. Preliminaries

Contrastive Representation Learning. Contrastive learning aims to structure an embedding space by attracting semantically related samples, which form positive pairs, and repelling unrelated ones, which constitute negative pairs. Formally, let $\mathbf{z}_i = f_\theta(\mathbf{h}_i)$ be the representation of an input \mathbf{h}_i , where f_θ denotes the sub-network that computes this representation. Then, the InfoNCE loss can be defined as:

$$\mathcal{L}_{Cont} = -\log \frac{e^{\text{sim}(\mathbf{z}_i, \mathbf{z}_i^+)/\tau}}{\sum_j e^{\text{sim}(\mathbf{z}_i, \mathbf{v}_j)/\tau}} \quad (1)$$

where $(\mathbf{z}_i, \mathbf{z}_i^+)$ denotes a positive pair, where \mathbf{z}_i^+ is an augmented view of \mathbf{z}_i obtained through data augmentation. The term $\text{sim}(\mathbf{z}_i, \mathbf{z}_j) = \mathbf{z}_i^\top \cdot \mathbf{z}_j / (\|\mathbf{z}_i\|_2 \cdot \|\mathbf{z}_j\|_2)$ represents the cosine similarity between two vectors. τ is a temperature hyperparameter, which we set to 1 for simplicity.

Dispersive Loss The core principle of Dispersive Loss is to enforce mutual repulsion among feature representations within the latent space. This effect is analogous to negative sample repulsion in self-supervised contrastive learning. Diverging from conventional contrastive methods, Dispersive Loss is formulated as a positive-pair-free contrastive objective. This design is predicated on the assumption that the primary generative task, governed by the diffusion objective \mathcal{L}_{Diff} , already provides a sufficient alignment signal. Therefore, the Dispersive Loss \mathcal{L}_{Disp} is incorporated as an auxiliary regularization term alongside the standard training objective of the diffusion model. For a given data batch $X = \{x_i\}$, the total loss is defined as:

$$\mathcal{L}(X) = \mathbb{E}_{x_i \in X} [\mathcal{L}_{Diff}(x_i)] + \lambda \mathcal{L}_{Disp}(X) \quad (2)$$

where the dispersive loss \mathcal{L}_{Disp} is computed over the entire mini-batch, where λ is a hyperparameter that controls the trade-off between the regression objective and the regularization strength. Within the InfoNCE framework, the dispersive loss discards the alignment term for positive pairs, exclusively retaining the repulsion term across arbitrary sample pairs, which can be formulated as:

$$\mathcal{L}_{Disp} = \log \mathbb{E}_{i,j} [e^{-\text{sim}(\mathbf{z}_i, \mathbf{z}_j)/\tau}] \quad (3)$$

where $\text{sim}(\cdot, \cdot)$ means the similarity metric function.

4. Repulsor

Given a mini-batch VAE latent images $\mathbf{X} = \{\mathbf{x}_i\}$, we first sample a diffusion timestep $t \sim \text{Uniform}\{1, \dots, T\}$. Then, the diffusion forward process can be written as:

$$\mathbf{x}_t = \sqrt{\bar{\alpha}_t} \mathbf{x}_0 + \sqrt{1 - \bar{\alpha}_t} \boldsymbol{\epsilon}, \quad \boldsymbol{\epsilon} \sim \mathcal{N}(\mathbf{0}, \mathbf{I}), \quad \bar{\alpha}_t = \prod_{s=1}^t (1 - \beta_s) \quad (4)$$

where \mathbf{x}_0 is the clean latent and \mathbf{x}_t is the noised latent. α and β are pre-defined hyper-parameters. Then the corresponding timestep t and noisy latent \mathbf{x}_t will be fed into SiT models to yield intermediate features $\mathbf{H}_t = \{\mathbf{h}_i\}_{i=1}^B$:

$$\mathbf{h}_b = f_{SiT[1:F_l]}(\mathbf{x}_t, e_t) \quad (5)$$

where $f_{SiT[1:F_l]}$ means the first F_l blocks of SiT model. Subsequently, a single-layer linear projection head, g_θ , is

Algorithm 1 Repulsor training in PyTorch-like style.

```

# f: encoder networks
# queue: dictionary as a queue of K keys (CxK)
# tgt: target layer for disperse loss
# m: momentum
# t: temperature
# gamma: loss weight

opt = AdamW(f.parameters()) # # Setup optimizer

# load a minibatch x and label y with N samples
for x, y in loader:
    x_n = VAE(x) # to latent space + normalize latents
    # iterate over f layers
    for i in range(len(self.blocks)):
        # choose one layer
        q = f.blocks[i](x_n)
        # target layer tgt for computing l_disp
        if i == tgt:
            # linear projection of q
            k = linear_proj(q.view(q.size(0), -1))

            # enqueue the current minibatch
            enqueue(queue, k)
            # dequeue the earliest minibatch
            dequeue(queue)

            # pairwise squared Euclidean distances
            dist = cdist(k, queue.T.detach(), p=2) ** 2
            # disperse loss, Eqn.(7)
            l_disp = log(mean(exp(-dist / t)))

        # compute the conditioned model prediction
        y_pred = f.forward(x_n, y)
        # diffusion loss
        l_diff = mean((y_pred - y) ** 2)
        # total loss calculation
        loss = l_diff + gamma * l_disp

    # SGD update
    opt.zero_grad()
    loss.backward()
    opt.step()

```

employed to map the high-dimensional features \mathbf{h}_b into a D -dimensional latent space, producing the final latent representations $\mathbf{Z}_t = \{\mathbf{z}_i\}_{i=1}^B$, which can be written as:

$$\mathbf{z}_i = \text{norm}(g_\theta(\mathbf{h}_i)) \in \mathbb{R}^D \quad (6)$$

where $\text{norm}(\cdot)$ denotes the L_2 normalization. To increase the number of negative pairs, we construct a memory bank $\mathcal{M} = \{\mathbf{m}_i\}_{i=1}^K$ as a queue of size K , where $\mathbf{m}_i \in \mathbb{R}^{1 \times D}$ is the i -th negative sample. Similar to Moco [24], the memory bank is updated by the First-In, First-Out policy. Then, the dispersive objective of current batch can be written as:

$$\mathcal{L}_{Disp} = \log \frac{1}{BK} \sum_{i=1}^B \sum_{k=1}^K \exp \left(-\frac{D_{ik}}{\tau} \right) \quad (7)$$

where $D_{ik} = \|\mathbf{z}_i - \text{sg}(\mathbf{m}_k)\|_2^2$ is defined as the squared Euclidean distance and $\text{sg}(\cdot)$ denotes the stop-gradient operation. After calculating the dispersive loss, we fed the latent representation \mathbf{Z}_t into the remaining part of SiT model $f_{SiT[F_l:F_f]}$, where F_f is total the number of blocks of SiT model to yield noise prediction \hat{e} to calculate diffusion loss.

Finally, we formulate the overall training objective as a

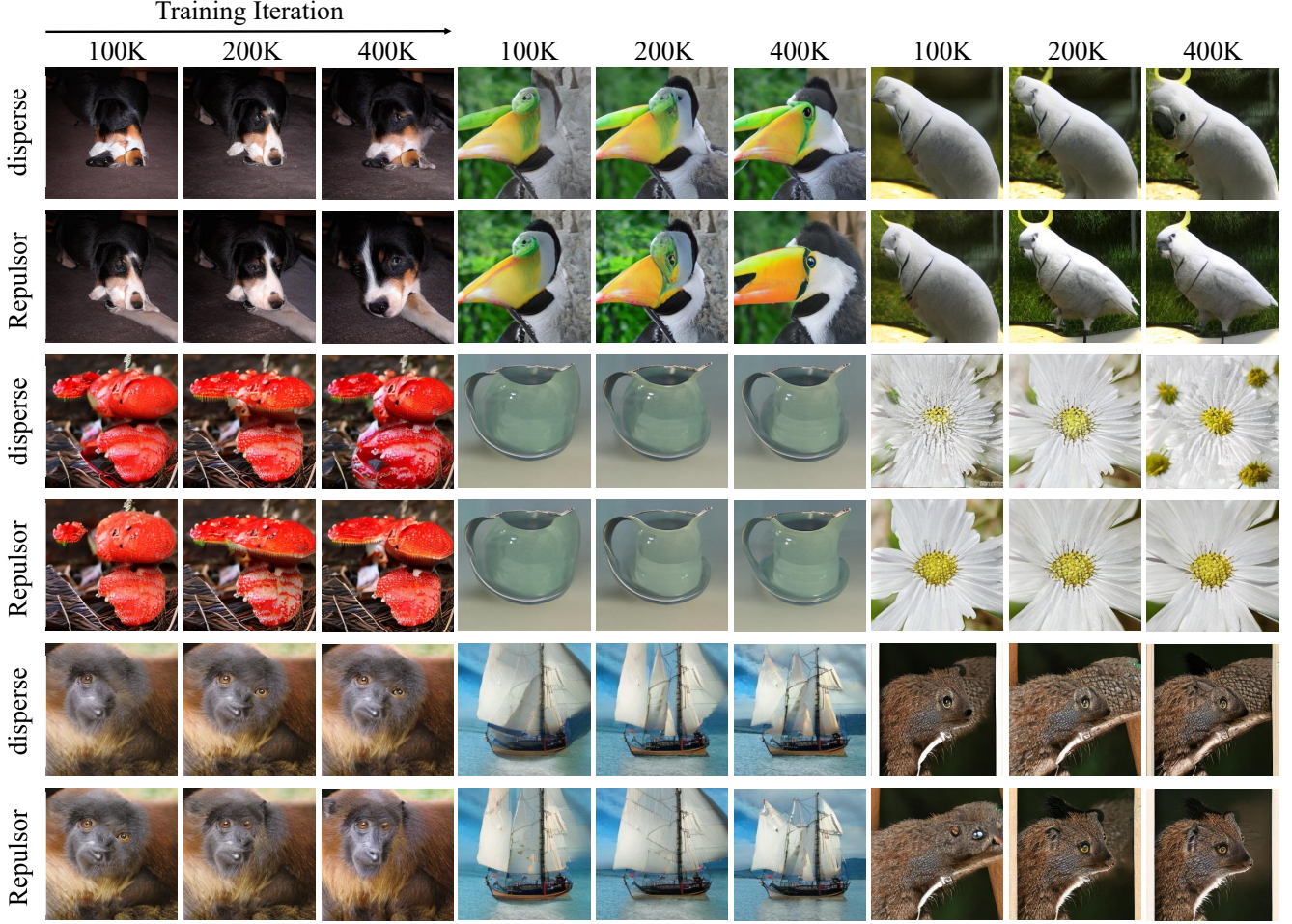


Figure 3. Generated Image Comparison of Repulsor vs disperse [55]. To evaluate the effect of disperse and Repulsor, we compare images generated by two SiT-XL/2 models during the first 400K training iterations. For a fair comparison, both models are run without classifier-free guidance with $\omega = 1.5$ and share the exact same initial noise, sampler, and number of sampling steps.

weighted sum of the diffusion loss and the disperse loss:

$$\mathcal{L} = \mathcal{L}_{Diff} + \gamma \cdot \mathcal{L}_{Disp} \quad (8)$$

where γ is a hyperparameter that balances the disperse and diffusion loss. The memory bank and the projection head are introduced as auxiliary modules exclusively for the optimization process during training. At inference time, these modules are detached, ensuring the efficiency of Repulsor. Algorithm 1 presents the pre-training pseudocode.

5. Experimental

Implementation details. Our experiments adopt the SiT [39] architecture, and the original model serves as our primary baseline. To ensure a fair comparison, we strictly adhere to the implementation settings from [39, 55] and conduct our evaluations on ImageNet [13] at a fixed 256×256 resolution. The training is performed in a $32 \times 32 \times 4$ latent

space encoded by a VAE tokenizer [47]. For optimization, we employ the AdamW optimizer [38] with a learning rate of 1×10^{-4} , $(\beta_1, \beta_2) = (0.9, 0.95)$, and with no weight decay. During the sampling phase, we use an ODE-based Heun sampler with 250 fixed steps, consistent with [39, 55]. All experiments were conducted on 8 A100 (80GB) GPUs. The configuration details can be found in Appendix 7.

Comparison methods. In experiments evaluating Repulsor under CFG, we benchmark against a diverse suite of recent diffusion-based generative models that vary in input parameterizations and architectural design. Specifically, we consider four families: (a) pixel-space diffusion, including ADM-U [15], VDM++ [30], and Simple Diffusion [28]; (b) Transformer-based latent diffusion, covering U-ViT [3], DiffiT [23], DiT [43], and SiT [39]; (c) masked diffusion transformers, represented by MaskDiT [64] and MDTv2 [20]; and (d) approaches that leverage external pretrained encoders for representation alignment, including

Table 1. Performance comparison of Repulsor, disperse, and SiT under the classifier-free guidance-free setting. The results show that SiT integrated with Repulsor achieves the best performance. \dagger : applied to the single best block. \ddagger : applied to all blocks.

ImageNet 256×256, w/o cfg			
Model	Iter.	FID \downarrow	Δ
SiT-S/2	400K	60.63	-
SiT-S/2+dispersive	400K	58.45	-2.18 (-3.60%)
SiT-S/2+Repulsor	400K	54.36	-6.27 (-10.34%)
SiT-B/2	400K	36.49	-
SiT-B/2+dispersive \dagger	400K	32.35	-4.14 (-11.35%)
SiT-B/2+dispersive \ddagger	400K	32.05	-4.44 (-12.17%)
SiT-B/2+Repulsor	400K	27.46	-9.03 (-24.75%)
SiT-L/2	400K	20.41	-
SiT-L/2+dispersive	400K	16.68	-3.73 (-18.27%)
SiT-L/2+Repulsor	400K	16.43	-3.98 (-19.50%)
SiT-XL/2	400K	18.46	-
SiT-XL/2+dispersive	400K	15.95	-2.51 (-13.6%)
SiT-XL/2+Repulsor	400K	10.91	-7.55 (-40.9%)
SiT-XL/2	700K	14.06	-
SiT-XL/2+dispersive	700K	12.08	-1.98 (-14.1%)
SiT-XL/2+Repulsor	700K	9.93	-4.13 (-29.4%)
SiT-XL/2	1000K	12.18	-
SiT-XL/2	2000K	10.11	-
SiT-XL/2+dispersive	1000K	10.64	-1.54 (-12.6%)
SiT-XL/2+Repulsor	1000K	9.07	-3.11 (-25.5%)

REPA [60], U-REPA [54], and SARA [7].

5.1. Main Results

We present a comprehensive evaluation of various SiT models trained with Repulsor. All models, except SiT-XL/2, were trained for 400k iterations. Across all experiments, we uniformly set the hyperparameters to $\gamma = 0.25$ and $\tau = 0.5$. For SiT-XL/2, we comparatively analyze its performance with and without Classifier-Free Guidance (CFG), providing both quantitative evaluations and a qualitative assessment of the generated samples. In the following experiments, our results are compared against the SiT performance reported in disperse [55].

w/o CFG. As detailed in Table 1, in the absence of CFG, our proposed method, Repulsor, consistently outperforms disperse by achieving a lower Fréchet Inception Distance (FID; [26]) score throughout the entire training process on the SiT-XL/2 configuration. Notably, at just 400k iterations, Repulsor achieves an FID of 10.91, a score that is not only superior to disperse at 700k iterations (FID=12.08) but also surpasses the SiT baseline after 1M iterations. This represents a substantial improvement in training efficiency, reducing computational time by over 60%. Furthermore, Fig-

Table 2. FID comparisons based on classifier-free guidance using SiT-XL/2 backbone. Repulsor achieves comparable performance in only 80 epochs when compared to the 400 epochs for mini-batch disperse [55], yielding an approximately $5\times$ speed-up in convergence while attaining a slightly lower FID.

ImageNet 256×256, w/ cfg		
Model	Epochs	FID \downarrow
<i>Pixel diffusion</i>		
ADM-U [15]	400	3.94
VDM++ [30]	560	2.40
Simple diffusion [28]	800	2.77
<i>Latent Diffusion Transformer</i>		
U-ViT-H/2 [3]	240	2.29
DiffiT [23]	-	1.73
DiT-XL/2 [43]	1400	2.27
SiT-XL/2 [39]	200	3.30
SiT-XL/2 [39]	800	2.46
SiT-XL/2 [39]	1400	2.06
<i>Masked Diffusion Transformer</i>		
MaskDiT [64]	1600	2.28
MDTv2-XL/2 [20]	1080	1.58
<i>Representation Alignment</i>		
SiT-XL/2 + REPA [60]	800	1.42
SiT-XL/2 + U-REPA [54]	400	1.41
SiT-XL/2 + SARA [7]	400	1.36
<i>Dispersion Regularization</i>		
SiT-XL/2 +disperse [55]	40	7.32
SiT-XL/2 +disperse [55]	80	5.09
SiT-XL/2 +disperse [55]	140	3.42
SiT-XL/2 +Repulsor (Ours)	40	3.25
SiT-XL/2 +disperse [55]	200	2.90
SiT-XL/2 +Repulsor (Ours)	80	2.40

ure 3 presents a qualitative comparison at different training stages, initialized with the same noise vector. The results visually demonstrate that the model trained with Repulsor exhibits a more favorable evolutionary trajectory, consistently generating higher-quality images at all evaluated stages.

w/ CFG. We further conduct a quantitative evaluation of the SiT-XL/2 architecture under CFG. Our approach is benchmarked against several recent representative diffusion models across multiple metrics. To ensure a fair comparison, we adhere to the experimental setup of disperse and SiT, employing a fixed guidance scale of $w = 1.5$ without any hyperparameter fine-tuning. As presented in Table 2, Repulsor demonstrates remarkable training efficiency. It achieves performance comparable to disperse trained for 400 epochs with only 80 training epochs, a five-fold reduction in training cost. Moreover, Repulsor surpasses the orig-

Table 3. **Ablation Study on Regularization Block Placement on SiT-B/2.** We apply Repulsor to different blocks and measure the FID. The results clearly demonstrate that the proposed loss significantly improves generation quality in all tested settings. †: applied to the single best block. ‡: applied to all blocks.

Model	FID \downarrow	Δ
SiT-B/2	36.49	-
SiT-B/2+dispersive†	32.35	-4.14 (-11.35%)
SiT-B/2+dispersive‡	32.05	-4.44 (-12.17%)
block 6	33.37	-3.12 (-8.55%)
block 7	32.20	-4.29 (-11.76%)
block 8	27.46	-9.03 (-24.75%)
block 9	30.85	-5.64 (-15.46%)
block 10	29.55	-6.94 (-19.02%)
block 11	29.79	-6.70 (-18.36%)
block 12	34.21	-2.28 (-6.25%)

Table 4. FID scores of SiT-B/2 on ImageNet with varying down-sampling types. “Use projection” means whether to use projector in the latent space. “#Arch” means the architecture of projection. “Avg Pool to D ” means performing spatial pooling to D dimension. “Lin. to D ” means concatenating all patches to obtain $1 \times PD$ tensor, followed by a linear layer to obtain $1 \times D$ token.

Method	Use projection?	# Arch.	FID \downarrow
SiT [39]	✗	-	36.49
Repulsor	✓	Avg Pool to D	36.70
Repulsor (Ours)	✓	Lin. to D	32.88

inal SiT-XL/2 with only one-tenth the training epochs.

5.2. Ablation Study

Effect of Regularization Block. Setups. For the SiT-B/2 architecture, we apply the Repulsor regularization to only a single Transformer block, while all other training and evaluation configurations are kept identical to the baseline. **Results.** As demonstrated in Table 3, Repulsor yields significant performance improvements across all placement positions. Remarkably, applying Repulsor to just a single block alone surpasses the performance of applying the Dispersive regularizer to all blocks. This finding further corroborates the superior regularization capability of Repulsor and its ability to achieve higher generation quality.

Effect of Linear Projection. Setups. Using the SiT-B/2 backbone, we compare the SiT [39] (no projector) against two projector architectures: “Avg Pool to D ” and our proposed “Lin. to D ”, as detailed in Table 4. All other configurations remain consistent. **Results.** As shown in Table 4, the SiT baseline (FID 36.49) suffers from overfitting when using high-dimensional representations, and the “Avg Pool to D ” (FID 36.70) offers no improvement. Our pro-

Table 5. FID scores of SiT-B/2 on ImageNet with varying memory bank sizes. “no memory bank” means treating samples in the same mini-batch as negatives. “Num. Negatives” means the number of negative samples, i.e., memory bank size K .

Method	Batch Size	Memory Bank	Num. Negatives	FID \downarrow
disperse [55]	256	✗	-	32.88
Repulsor (Ours)	256	✓	65536	32.64
Repulsor (Ours)	256	✓	131072	27.46
Repulsor (Ours)	256	✓	262144	34.79

posed “Lin. to D ” projector, however, creates an effective information bottleneck that suppresses noise and reduces overhead. This method achieves the best FID of 32.88, significantly outperforming both alternatives.

Effect of CFG ratio. Setups. We analyze the effect of the CFG ratio w on generation quality on SiT-XL/2 under two distinct training budgets, 400k and 2000k steps. The evaluation is conducted using four standard metrics: FID, spatial FID (sFID; [40]), Precision [32], and Inception Score (IS; [49]). We provide more details of each metric in Appendix 8. **Results.** We observe that the FID score exhibits a characteristic U-shaped curve as a function of w , consistently reaching its optimum at approximately $w = 1.5$. In contrast, sFID shows a monotonic decrease with increasing w , while the Inception Score monotonically increases. Precision also demonstrates an overall improvement trend, indicating that stronger guidance yields sharper samples with higher class consistency. Mechanistically, a larger w amplifies the differential between the conditional and unconditional paths, steering the generation more closely toward the condition, yet simultaneously elevating the risk of mode collapse and distributional shift.

Effect of Memory Bank Size. Setups. We investigate the impact of varying memory bank sizes, denoted by K , on the SiT-B/2 architecture. We also include **disperse**, which serves as a “no memory bank” ablation (i.e., $K = 0$) where negative samples are drawn exclusively from the current mini-batch. All other training configurations remain consistent with our main experiments. **Results.** As presented in Table 5, the memory bank size significantly influences performance. The optimal FID score of 27.46 is achieved with $K = 131072$, outperforming both disperse and other memory configurations. An excessively large memory bank can dilute the contribution of in-batch hard negatives, reducing the gradient’s sensitivity to informative samples, which in turn weakens regularization and leads to performance degradation. Conversely, a memory bank that is too small or absent provides an insufficient approximation of the true data distribution, limiting generalization and failing to maintain a stable dispersion intensity.

Effect of Training Steps. Setups. We compare Repulsor against the baseline on two SiT architectures (SiT-B/2 and SiT-XL/2). **Results.** As shown in Figure 5, on

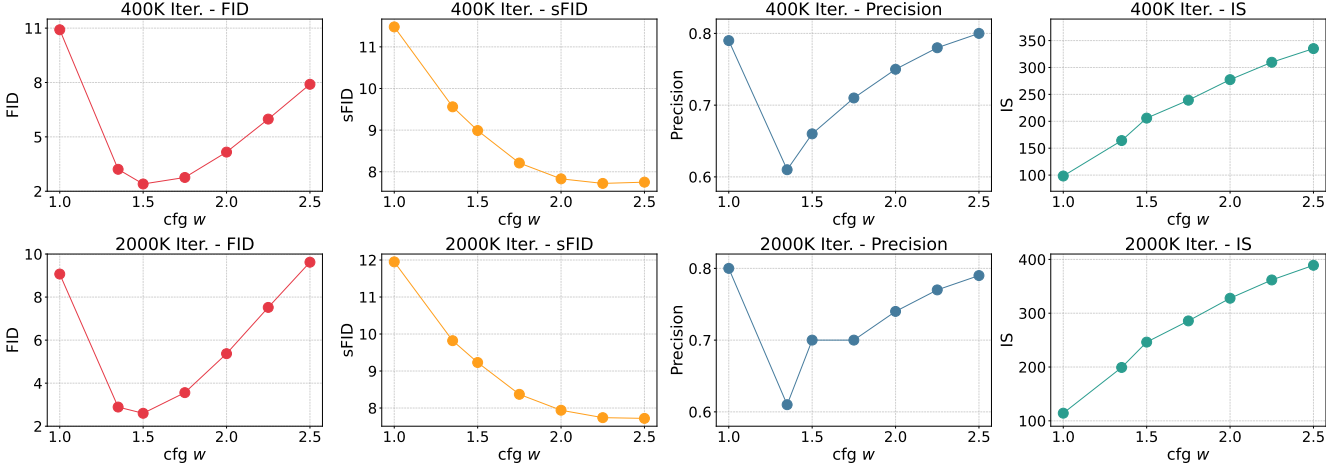


Figure 4. Impact of the CFG ratio w on generation quality. The eight subplots illustrate four metrics ($\text{FID}\downarrow$, $\text{sFID}\downarrow$, $\text{Precision}\uparrow$, and $\text{IS}\uparrow$) as a function of w at two different training checkpoints, namely 400K and 2000K iterations.

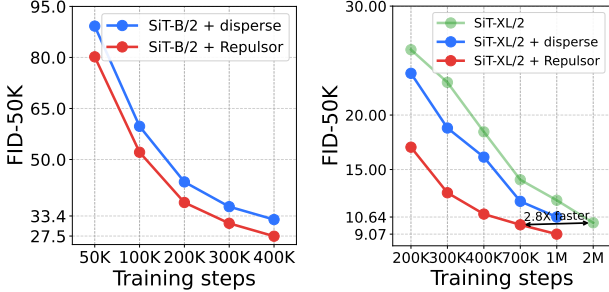


Figure 5. **Effectiveness of Repulsor on SiT with different architectures (SiT-B/2 on the left and SiT-XL/2 on the right).** We plot the FID-50k score on the ImageNet 256×256 dataset as a function of the training iterations. Compared to disperse, Repulsor consistently attains a lower FID score with considerably fewer iterations, demonstrating a significant improvement in both the training efficiency and generation quality of diffusion models.

the SiT-B/2 architecture, Repulsor consistently achieves a lower FID throughout the training process, yielding an average relative improvement of approximately 13.1%. On the larger SiT-XL/2 architecture, the advantages of Repulsor become more pronounced. To achieve an FID score below 11, Repulsor requires only 400K training steps (FID=10.91), whereas disperse necessitates 1M steps (FID=10.64). Furthermore, Repulsor demonstrates significantly enhanced sample efficiency. To achieve a comparable FID score, Repulsor requires only 700K steps (FID=9.93), whereas the original SiT model needs approximately 2M steps (FID=10.11). This demonstrates that Repulsor enhances sample efficiency by nearly 2.8×. When pushing performance further, Repulsor attains an even stronger score of 9.07 within just 1M steps. These results indicate that the performance gains from Repulsor

Table 6. Sensitivity analysis on τ and γ . We evaluate the performance of SiT-XL/2 on Repulsor with varying temperature τ and loss weight γ . All configurations outperform disperse.

Method	Temperature τ	Loss weight γ	FID \downarrow	Inception score \uparrow
SiT-XL/2 [39]	-	-	18.46	73.9
Repulsor	0.25	0.25	12.49	88.1
	0.25	0.5	11.40	88.9
	0.5	0.25	10.91	98.3

are particularly significant during the early-to-mid stages of training and are further amplified on larger-scale models.

Effect of τ , γ . Setup. We further investigate the two key hyperparameters in our loss function: the temperature τ and the regularization strength γ . We employ SiT-XL/2 and examine the impact of varying τ and γ on performance under the standard 400k-iteration training setting. **Results.** The results are presented in Table 6. We observe that the model achieves optimal performance with $\tau = 0.5$ and $\gamma = 0.25$. While an exhaustive grid search was computationally prohibitive, this parameter combination demonstrated robust and optimal performance within our explored range.

6. Conclusion

We present Repulsor, a simple yet effective regularization method designed to disperse the internal representations of a model. We investigate whether the size of the negative set in generative models follows a scaling law and evaluate its impact on representation quality. Experiments demonstrate that Repulsor significantly improves generative performance and accelerates convergence by dynamically maintaining a memory-efficient queue of negative samples, without requiring any additional data or pre-training. Our work provides new insights and strong empirical evidence

for dispersion regularization in generative models.

Limitation. While Repulsor significantly enhances the representation quality of generative models, its application to large-scale datasets like ImageNet reveals a potential challenge. These datasets are characterized by a high density of semantically similar instances, which can lead Repulsor to enforce an excessive separation between them in the feature space. This over-separation risks corrupting the global semantic structure of the learned representations. Consequently, the size of the memory bank emerges as a critical hyperparameter that dictates the final performance.

References

- [1] Mustafa Sercan Amac, Ahmet Sencan, Bugra Baran, Nazli Ikizler-Cinbis, and Ramazan Gokberk Cinbis. Masksplit: Self-supervised meta-learning for few-shot semantic segmentation. In *Proceedings of the IEEE/CVF winter conference on applications of computer vision*, pages 1067–1077, 2022. [3](#)
- [2] Alexei Baevski, Wei-Ning Hsu, Qiantong Xu, Arun Babu, Jiatao Gu, and Michael Auli. Data2vec: A general framework for self-supervised learning in speech, vision and language. In *International conference on machine learning*, pages 1298–1312. PMLR, 2022. [3](#)
- [3] Fan Bao, Shen Nie, Kaiwen Xue, Yue Cao, Chongxuan Li, Hang Su, and Jun Zhu. All are worth words: A vit backbone for diffusion models. In *IEEE/CVF Conference on Computer Vision and Pattern Recognition, CVPR 2023, Vancouver, BC, Canada, June 17-24, 2023*, pages 22669–22679. IEEE, 2023. [5](#), [6](#)
- [4] Hangbo Bao, Li Dong, Songhao Piao, and Furu Wei. Beit: Bert pre-training of image transformers. *arXiv preprint arXiv:2106.08254*, 2021. [2](#)
- [5] Tim Brooks, Bill Peebles, Connor Holmes, Will DePue, Yufei Guo, Li Jing, David Schnurr, Joe Taylor, Troy Luhman, Eric Luhman, et al. Video generation models as world simulators, 2024. [2](#), [3](#)
- [6] Mathilde Caron, Ishan Misra, Julien Mairal, Priya Goyal, Piotr Bojanowski, and Armand Joulin. Unsupervised learning of visual features by contrasting cluster assignments. *Advances in neural information processing systems*, 33:9912–9924, 2020. [2](#)
- [7] Hesen Chen, Junyan Wang, Zhiyu Tan, and Hao Li. Sara: Structural and adversarial representation alignment for training-efficient diffusion models. *arXiv preprint arXiv:2503.08253*, 2025. [2](#), [3](#), [6](#)
- [8] Ricky TQ Chen, Yulia Rubanova, Jesse Bettencourt, and David K Duvenaud. Neural ordinary differential equations. *Advances in neural information processing systems*, 31, 2018. [3](#)
- [9] Ting Chen, Simon Kornblith, Mohammad Norouzi, and Geoffrey Hinton. A simple framework for contrastive learning of visual representations. In *Proceedings of the 37th International Conference on Machine Learning. JMLR.org*, 2020. [2](#), [3](#)
- [10] Xinlei Chen and Kaiming He. Exploring simple siamese representation learning. In *Proceedings of the IEEE/CVF conference on computer vision and pattern recognition*, pages 15750–15758, 2021. [2](#)
- [11] Xiaokang Chen, Mingyu Ding, Xiaodi Wang, Ying Xin, Shentong Mo, Yunhao Wang, Shumin Han, Ping Luo, Gang Zeng, and Jingdong Wang. Context autoencoder for self-supervised representation learning. *International Journal of Computer Vision*, 132(1):208–223, 2024. [2](#)
- [12] Quan Dao, Hao Phung, Binh Nguyen, and Anh Tran. Flow matching in latent space. *arXiv preprint arXiv:2307.08698*, 2023. [3](#)
- [13] Jia Deng, Wei Dong, Richard Socher, Li-Jia Li, Kai Li, and Li Fei-Fei. ImageNet: A large-scale hierarchical image database. In *2009 IEEE conference on computer vision and pattern recognition*, pages 248–255. Ieee, 2009. [5](#)
- [14] Prafulla Dhariwal and Alexander Nichol. Diffusion models beat gans on image synthesis. *Advances in neural information processing systems*, 34:8780–8794, 2021. [2](#), [3](#)
- [15] Prafulla Dhariwal and Alexander Quinn Nichol. Diffusion models beat gans on image synthesis. In *Advances in Neural Information Processing Systems 34: Annual Conference on Neural Information Processing Systems 2021, NeurIPS 2021, December 6-14, 2021, virtual*, pages 8780–8794, 2021. [5](#), [6](#)
- [16] Laurent Dinh, Jascha Sohl-Dickstein, and Samy Bengio. Density estimation using real nvp. *arXiv preprint arXiv:1605.08803*, 2016. [3](#)
- [17] Xiaoyi Dong, Jianmin Bao, Ting Zhang, Dongdong Chen, Weiming Zhang, Lu Yuan, Dong Chen, Fang Wen, Nenghai Yu, and Baining Guo. Poco: Perceptual codebook for bert pre-training of vision transformers. In *Proceedings of the AAAI conference on artificial intelligence*, pages 552–560, 2023. [3](#)
- [18] Patrick Esser, Sumith Kulal, Andreas Blattmann, Rahim Entezari, Jonas Müller, Harry Saini, Yam Levi, Dominik Lorenz, Axel Sauer, Frederic Boesel, et al. Scaling rectified flow transformers for high-resolution image synthesis. In *Forty-first International Conference on Machine Learning*, 2024. [2](#), [3](#)
- [19] Johannes S Fischer, Ming Gui, Pingchuan Ma, Nick Stracke, Stefan A Baumann, and Björn Ommer. Boosting latent diffusion with flow matching. *arXiv preprint arXiv:2312.07360*, 2023. [2](#), [3](#)
- [20] Shanghua Gao, Pan Zhou, Ming-Ming Cheng, and Shuicheng Yan. Mdtv2: Masked diffusion transformer is a strong image synthesizer, 2024. [5](#), [6](#)
- [21] Jean-Bastien Grill, Florian Strub, Florent Altché, Corentin Tallec, Pierre Richemond, Elena Buchatskaya, Carl Doersch, Bernardo Avila Pires, Zhaohan Guo, Mohammad Gheshlaghi Azar, et al. Bootstrap your own latent-a new approach to self-supervised learning. *Advances in neural information processing systems*, 33:21271–21284, 2020. [2](#)
- [22] Yuwei Guo, Ceyuan Yang, Anyi Rao, Zhengyang Liang, Yaohui Wang, Yu Qiao, Maneesh Agrawala, Dahua Lin, and Bo Dai. Animatediff: Animate your personalized text-to-image diffusion models without specific tuning. *arXiv preprint arXiv:2307.04725*, 2023. [3](#)

[23] Ali Hatamizadeh, Jiaming Song, Guilin Liu, Jan Kautz, and Arash Vahdat. Diffit: Diffusion vision transformers for image generation. *CoRR*, abs/2312.02139, 2023. 5, 6

[24] Kaiming He, Haoqi Fan, Yuxin Wu, Saining Xie, and Ross Girshick. Momentum contrast for unsupervised visual representation learning. In *Proceedings of the IEEE/CVF conference on computer vision and pattern recognition*, pages 9729–9738, 2020. 2, 4

[25] Kaiming He, Xinlei Chen, Saining Xie, Yanghao Li, Piotr Dollár, and Ross Girshick. Masked autoencoders are scalable vision learners. In *Proceedings of the IEEE/CVF conference on computer vision and pattern recognition*, pages 16000–16009, 2022. 2, 3

[26] Martin Heusel, Hubert Ramsauer, Thomas Unterthiner, Bernhard Nessler, and Sepp Hochreiter. Gans trained by a two time-scale update rule converge to a local nash equilibrium. *Advances in neural information processing systems*, 30, 2017. 6, 1

[27] Jonathan Ho, Ajay Jain, and Pieter Abbeel. Denoising diffusion probabilistic models. *Advances in neural information processing systems*, 33:6840–6851, 2020. 2, 3

[28] Emiel Hoogeboom, Jonathan Heek, and Tim Salimans. simple diffusion: End-to-end diffusion for high resolution images. In *International Conference on Machine Learning, ICML 2023, 23-29 July 2023, Honolulu, Hawaii, USA*, pages 13213–13232. PMLR, 2023. 5, 6

[29] Li Hu. Animate anyone: Consistent and controllable image-to-video synthesis for character animation. In *Proceedings of the IEEE/CVF Conference on Computer Vision and Pattern Recognition (CVPR)*, pages 8153–8163, 2024. 2, 3

[30] Diederik P. Kingma and Ruiqi Gao. Understanding diffusion objectives as the ELBO with simple data augmentation. In *Advances in Neural Information Processing Systems 36: Annual Conference on Neural Information Processing Systems 2023, NeurIPS 2023, New Orleans, LA, USA, December 10 - 16, 2023*, 2023. 5, 6

[31] Soroush Abbasi Koohpayegani, Ajinkya Tejankar, and Hamed Pirsiavash. Mean shift for self-supervised learning. In *Proceedings of the IEEE/CVF International Conference on Computer Vision*, pages 10326–10335, 2021. 2

[32] Tuomas Kynkänniemi, Tero Karras, Samuli Laine, Jaakko Lehtinen, and Timo Aila. Improved precision and recall metric for assessing generative models. 2019. 7, 1

[33] Matthew Le, Apoorv Vyas, Bowen Shi, Brian Karrer, Leda Sari, Rashed Moritz, Mary Williamson, Vimal Manohar, Yossi Adi, Jay Mahadeokar, et al. Voicebox: Text-guided multilingual universal speech generation at scale. *Advances in neural information processing systems*, 36, 2024. 2, 3

[34] Jaa-Yeon Lee, Byunghee Cha, Jeongsol Kim, and Jong Chul Ye. Aligning text to image in diffusion models is easier than you think. *arXiv preprint arXiv:2503.08250*, 2025. 2, 3

[35] Xingjian Leng, Jaskirat Singh, Yunzhong Hou, Zhenchang Xing, Saining Xie, and Liang Zheng. Repa-e: Unlocking vae for end-to-end tuning with latent diffusion transformers. *arXiv preprint arXiv:2504.10483*, 2025. 2, 3

[36] Yaron Lipman, Ricky TQ Chen, Heli Ben-Hamu, Maximilian Nickel, and Matt Le. Flow matching for generative modeling. *arXiv preprint arXiv:2210.02747*, 2022. 2, 3

[37] Xingchao Liu, Chengyue Gong, and Qiang Liu. Flow straight and fast: Learning to generate and transfer data with rectified flow. *arXiv preprint arXiv:2209.03003*, 2022. 2, 3

[38] Ilya Loshchilov and Frank Hutter. Decoupled weight decay regularization. *arXiv preprint arXiv:1711.05101*, 2017. 5

[39] Nanye Ma, Mark Goldstein, Michael S Albergo, Nicholas M Boffi, Eric Vanden-Eijnden, and Saining Xie. SiT: Exploring flow and diffusion-based generative models with scalable interpolant transformers. In *European Conference on Computer Vision*, pages 23–40. Springer, 2024. 2, 5, 6, 7, 8

[40] Charlie Nash, Jacob Menick, Sander Dieleman, and Peter W Battaglia. Generating images with sparse representations. *arXiv preprint arXiv:2103.03841*, 2021. 7, 1

[41] Alexander Quinn Nichol and Prafulla Dhariwal. Improved denoising diffusion probabilistic models. In *International conference on machine learning*, pages 8162–8171. PMLR, 2021. 3

[42] Maxime Oquab, Timothée Darcret, Théo Moutakanni, Huy Q. Vo, Marc Szafraniec, Vasil Khalidov, Pierre Fernandez, Daniel Haziza, Francisco Massa, Alaaeldin El-Nouby, Mahmoud Assran, Nicolas Ballas, Wojciech Galuba, Russ Howes, Po-Yao (Bernie) Huang, Shang-Wen Li, Ishan Misra, Michael G. Rabbat, Vasu Sharma, Gabriel Synnaeve, Huijiao Xu, Hervé Jégou, Julien Mairal, Patrick Labatut, Armand Joulin, and Piotr Bojanowski. Dinov2: Learning robust visual features without supervision. *ArXiv*, abs/2304.07193, 2023. 2

[43] William Peebles and Saining Xie. Scalable diffusion models with transformers. In *Proceedings of the IEEE/CVF International Conference on Computer Vision*, pages 4195–4205, 2023. 2, 3, 5, 6

[44] Adam Polyak, Amit Zohar, Andrew Brown, Andros Tjandra, Animesh Sinha, Ann Lee, Apoorv Vyas, Bowen Shi, Chih-Yao Ma, Ching-Yao Chuang, et al. Movie gen: A cast of media foundation models. *arXiv preprint arXiv:2410.13720*, 2024. 3

[45] Aditya Ramesh, Prafulla Dhariwal, Alex Nichol, Casey Chu, and Mark Chen. Hierarchical text-conditional image generation with clip latents. *arXiv preprint arXiv:2204.06125*, 1 (2):3, 2022. 2, 3

[46] Danilo Rezende and Shakir Mohamed. Variational inference with normalizing flows. In *International conference on machine learning*, pages 1530–1538. PMLR, 2015. 3

[47] Robin Rombach, Andreas Blattmann, Dominik Lorenz, Patrick Esser, and Björn Ommer. High-resolution image synthesis with latent diffusion models. In *Proceedings of the IEEE/CVF conference on computer vision and pattern recognition*, pages 10684–10695, 2022. 2, 3, 5

[48] Chitwan Saharia, William Chan, Saurabh Saxena, Lala Li, Jay Whang, Emily L Denton, Kamyar Ghasemipour, Raphael Gontijo Lopes, Burcu Karagol Ayan, Tim Salimans, et al. Photorealistic text-to-image diffusion models with deep language understanding. *Advances in neural information processing systems*, 35:36479–36494, 2022. 2, 3

[49] Tim Salimans, Ian Goodfellow, Wojciech Zaremba, Vicki Cheung, Alec Radford, and Xi Chen. Improved techniques for training gans. *Advances in neural information processing systems*, 29, 2016. 7, 1

[50] Jiaming Song, Chenlin Meng, and Stefano Ermon. Denoising diffusion implicit models. *arXiv preprint arXiv:2010.02502*, 2020. 2, 3

[51] Yang Song, Jascha Sohl-Dickstein, Diederik P Kingma, Abhishek Kumar, Stefano Ermon, and Ben Poole. Score-based generative modeling through stochastic differential equations. *arXiv preprint arXiv:2011.13456*, 2020. 2, 3

[52] Christian Szegedy, Vincent Vanhoucke, Sergey Ioffe, Jon Shlens, and Zbigniew Wojna. Rethinking the Inception architecture for computer vision. In *CVPR*, 2016. 1

[53] Yonglong Tian, Dilip Krishnan, and Phillip Isola. Contrastive multiview coding. In *European conference on computer vision*, pages 776–794. Springer, 2020. 2

[54] Yuchuan Tian, Hanting Chen, Mengyu Zheng, Yuchen Liang, Chao Xu, and Yunhe Wang. U-repa: Aligning diffusion u-nets to vits. *arXiv preprint arXiv:2503.18414*, 2025. 2, 3, 6

[55] Runqian Wang and Kaiming He. Diffuse and disperse: Image generation with representation regularization. *arXiv preprint arXiv:2506.09027*, 2025. 2, 3, 5, 6, 7

[56] Chen Wei, Haoqi Fan, Saining Xie, Chao-Yuan Wu, Alan Yuille, and Christoph Feichtenhofer. Masked feature prediction for self-supervised visual pre-training. In *Proceedings of the IEEE/CVF conference on computer vision and pattern recognition*, pages 14668–14678, 2022. 3

[57] Zhenda Xie, Zheng Zhang, Yue Cao, Yutong Lin, Jianmin Bao, Zhuliang Yao, Qi Dai, and Han Hu. Simmim: A simple framework for masked image modeling. In *Proceedings of the IEEE/CVF conference on computer vision and pattern recognition*, pages 9653–9663, 2022. 2, 3

[58] Wanghan Xu, Xiaoyu Yue, Zidong Wang, Yao Teng, Wenlong Zhang, Xihui Liu, Luping Zhou, Wanli Ouyang, and Lei Bai. Exploring representation-aligned latent space for better generation. *arXiv preprint arXiv:2502.00359*, 2025. 2

[59] Jingfeng Yao, Bin Yang, and Xinggang Wang. Reconstruction vs. generation: Taming optimization dilemma in latent diffusion models. In *Proceedings of the IEEE/CVF Conference on Computer Vision and Pattern Recognition (CVPR)*, pages 15703–15712, 2025. 3

[60] Sihyun Yu, Sangkyung Kwak, Huiwon Jang, Jongheon Jeong, Jonathan Huang, Jinwoo Shin, and Saining Xie. Representation alignment for generation: Training diffusion transformers is easier than you think. *arXiv preprint arXiv:2410.06940*, 2024. 2, 3, 6

[61] Kaiwen Zha, Peng Cao, Jeany Son, Yuzhe Yang, and Dina Katabi. Rank-n-contrast: learning continuous representations for regression. *Advances in Neural Information Processing Systems*, 36:17882–17903, 2023. 2, 3

[62] Hao Zhang, Feng Li, Shilong Liu, Lei Zhang, Hang Su, Jun Zhu, Lionel M Ni, and Heung-Yeung Shum. Dino: Detr with improved denoising anchor boxes for end-to-end object detection. *arXiv preprint arXiv:2203.03605*, 2022. 2, 3

[63] Lvmin Zhang, Anyi Rao, and Maneesh Agrawala. Adding conditional control to text-to-image diffusion models. In *Proceedings of the IEEE/CVF International Conference on Computer Vision*, pages 3836–3847, 2023. 2, 3

[64] Hongkai Zheng, Weili Nie, Arash Vahdat, and Anima Anandkumar. Fast training of diffusion models with masked transformers. *Trans. Mach. Learn. Res.*, 2024, 2024. 5, 6

Repulsor: Accelerating Generative Modeling with a Contrastive Memory Bank

Supplementary Material

model	S/2	B/2	L/2	XL/2
model configurations				
params (M)	33	130	458	675
depth	12	12	24	28
hidden dim	384	768	1024	1152
patch size	2	2	2	2
heads	6	12	16	16
training configurations				
epochs	80	80	80	80 - 200
batch size		256		
optimizer		AdamW		
optimizer β_1		0.9		
optimizer β_2		0.95		
weight decay		0.0		
learning rate (lr)		1×10^{-4}		
lr schedule		constant		
lr warmup		none		
ODE sampling				
steps		250		
sampler		Heun		
t schedule		linear		
last step size		N/A		
Dispersive Loss				
regularization strength γ		0.25		
temperature τ		0.5		
memory bank size K	65536	131072	32768	32768

Table 7. SiT Configuration on ImageNet.

7. Additional Experimental Details

Our ImageNet experiments are run on 8 A100 (80GB) GPUs. We strictly adhere to the settings and codebase of the SiT paper. Specifically, we utilize the AdamW optimizer with a learning rate of 1×10^{-4} , $(\beta_1, \beta_2) = (0.9, 0.95)$, and zero weight decay. The ODE sampling is performed using a Heun solver with 250 steps. Complete configuration details are available in Table 7.

8. Evaluation Detail

We assess our method using several standard metrics:

- Fréchet Inception Distance (FID) [26]: This metric calculates the feature distance between the real and generated image distributions. It utilizes features extracted from the Inception-v3 network [52], assuming both feature sets follow a multivariate Gaussian distribution.
- Spatial FID (sFID) [40]: A variant of FID, sFID computes the distance using intermediate spatial features

from the Inception-v3 network, specifically to evaluate the spatial characteristics of the generated images.

- Precision [32]: Adapted from their classic definitions, precision measures the fraction of generated images considered realistic, while recall measures the fraction of the true data manifold covered by the generated distribution.
- Inception Score (IS) [49]: Also leveraging the Inception-v3 network, IS evaluates quality and diversity by measuring the KL-divergence between the conditional label distribution (derived from softmax-normalized logits) and the marginal label distribution.

9. More qualitative results



Figure 6. Uncurated generation results of SiT-XL/2+Repulsor. We use classifier-free guidance with $w = 4.0$. Class label=“goldfinch”(11).



Figure 7. Uncurated generation results of SiT-XL/2+Repulsor. We use classifier-free guidance with $w = 4.0$. Class label=“black swan”(100).



Figure 8. Uncurated generation results of SiT-XL/2+Repulsor. We use classifier-free guidance with $w = 4.0$. Class label=“sea anemone”(108).



Figure 9. Uncurated generation results of SiT-XL/2+Repulsor. We use classifier-free guidance with $w = 4.0$. Class label=“cairn”(192).



Figure 10. Uncurated generation results of SiT-XL/2+Repulsor. We use classifier-free guidance with $w = 4.0$. Class label=“arctic fox”(279).



Figure 11. Uncurated generation results of SiT-XL/2+Repulsor. We use classifier-free guidance with $w = 4.0$. Class label=“lesser panda”(387).



Figure 12. Uncurated generation results of SiT-XL/2+Repulsor. We use classifier-free guidance with $w = 4.0$. Class label=“puffer”(397).



Figure 13. Uncurated generation results of SiT-XL/2+Repulsor. We use classifier-free guidance with $w = 4.0$. Class label=“folding chair”(559).



Figure 14. Uncurated generation results of SiT-XL/2+Repulsor. We use classifier-free guidance with $w = 4.0$. Class label=“grand piano”(579).



Figure 15. Uncurated generation results of SiT-XL/2+Repulsor. We use classifier-free guidance with $w = 4.0$. Class label=“magnetic compass”(635).



Figure 16. Uncurated generation results of SiT-XL/2+Repulsor. We use classifier-free guidance with $w = 4.0$. Class label=“pot”(738).



Figure 17. Uncurated generation results of SiT-XL/2+Repulsor. We use classifier-free guidance with $w = 4.0$. Class label=“hot pot”(926).



Figure 18. Uncurated generation results of SiT-XL/2+Repulsor. We use classifier-free guidance with $w = 4.0$. Class label=“cheeseburger”(933).



Figure 19. Uncurated generation results of SiT-XL/2+Repulsor. We use classifier-free guidance with $w = 4.0$. Class label=“carbonara”(959).